SRG/ART-XC and NuSTAR observations of the X-Ray pulsar GRO J1008-57 in the lowest luminosity state

Lutovinov, A.; Tsygankov, S.; Molkov, S.; Doroshenko, V.; Mushtukov, A.; Arefiev, V.; ... ; Pavlinsky, M.

Draft version March 11, 2021
Typeset using LaTeX **twocolumn** style in AASTeX63

SRG/ART-XC and *NuSTAR* observations of the X-ray pulsar GRO J1008−57 in the lowest luminosity state

A. Lutovinov,[1] S. Tsygankov,[2,1] S. Molkov,[1] V. Doroshenko,[3,1] A. Mushtukov,[4,1,5] V. Arefiev,[1] I. Lapshov,[1] A. Tkachenko,[1] and M. Pavlinsky[1]

[1]*Space Research Institute, Russian Academy of Sciences, Profsoyuznaya 84/32, 117997 Moscow, Russia*
[2]*Department of Physics and Astronomy, FI-20014 University of Turku, Finland*
[3]*Institute for Astronomy and Astrophysics, University of Tübingen, Sand 1, 72026 Tübingen, Germany*
[4]*Leiden Observatory, Leiden University, NL-2300RA Leiden, The Netherlands*
[5]*Pulkovo Observatory, Russian Academy of Sciences, Saint Petersburg 196140, Russia*

(Received XXX, 2020; Revised XXX, 2020; Accepted XXX)

Submitted to ApJ

ABSTRACT

We report results of the first broadband observation of the transient X-ray pulsar GRO J1008−57 performed in the quiescent state. Observations were conducted quasi-simultaneously with the *Mikhail Pavlinsky* ART-XC telescope on board *SRG* and *NuSTAR* right before the beginning of a Type I outburst. GRO J1008−57 was detected in the state with the lowest observed luminosity around several $\times 10^{34}$ erg s^{-1} and consequently accreting from the cold disk. Timing analysis allowed to significantly detect pulsations during this state for the first time. The observed pulsed fraction of about 20% is, however, almost three times lower than in brighter states when the accretion proceeds through the standard disk. We traced the evolution of the broadband spectrum of the source on a scale of three orders of magnitude in luminosity and found that at the lowest luminosities the spectrum transforms into the double-hump structure similarly to other X-ray pulsars accreting at low luminosities (X Persei, GX 304–1, A 0535+262) reinforcing conclusion that this spectral shape is typical for these objects.

Keywords: pulsars: individual (GRO J1008−57) – stars: neutron – X-rays: binaries

1. INTRODUCTION

A significant progress in studies of strongly magnetized neutron stars in binary systems (a.k.a. X-ray pulsars, XRPs) has been made over the last years due to extraordinary technical capabilities of the currently operating X-ray observatories. As a result, the range of observable luminosities from such objects extended over nine orders of magnitude from $L_X \sim 10^{40} - 10^{41}$ erg s^{-1} for pulsating ultra luminous X-ray sources (Bachetti et al. 2014; Fürst et al. 2016; Israel et al. 2017; Rodríguez Castillo et al. 2020; Doroshenko et al. 2020) to $L_X \sim 10^{32} - 10^{33}$ erg s^{-1} for XRPs in quiescent state (see e.g., Campana et al. 2002; Doroshenko et al. 2014; Wijnands & Degenaar 2016; Tsygankov et al. 2017b), allowing to study absolutely different regimes of accretion onto highly magnetized neutron stars (NSs). In addition to the improved technical characteristics, the flexibility in arrangement for long-term monitoring campaigns played a major role. For instance, *Swift*/XRT data allowed to discover transitions of several XRPs to the propeller regime, caused by the centrifugal inhibition of accretion (see, e.g., Tsygankov et al. 2016; Lutovinov et al. 2017, 2019; Semena et al. 2019). For slower pulsars a new regime of the accretion, from a low-ionized (cold) accretion disk, was discovered (Tsygankov et al. 2017a). This regime is characterized by the transition of accretion to a quasi-stable state with the luminosity of the order of $L_X \sim 10^{34} - 10^{35}$ erg s^{-1}. Broadband observations of several pulsars at this low luminosity level demonstrated also a rather complex shape consisting of two components – a low-energy thermal component and a high-energy one, presumably associated with the cyclotron radiation (Tsygankov et al. 2019b,a; Mushtukov et al. 2020).

Since physics of interaction of the cold disk with the strong magnetic field of the NS is still unexplored, any additional observations in this state are of vital importance. The first pulsar where the accretion from the cold disk was discovered is GRO J1008−57, a long-period ($P \sim 94$ s) transient XRP in the binary system with the Be star as a normal companion

Corresponding author: A. Lutovinov
aal@iki.rssi.ru

Table 1. List of GRO J1008−57 observations utilized in this work.

ObsID	Start date	Start MJD	Exp. (ks)	$P_{\rm spin}$, s [a]
		NuSTAR		
80001001002	2012-11-30	56261.36	12.5	93.5727(2)
90001003002	2014-12-03	56994.81	22.3	93.4429(4)
90001003004	2015-01-27	57049.74	12.5	93.3606(2)
90401338002	2018-10-17	58408.67	45.3	93.2207(2)
90501357002	2020-01-01	58849.79	45.2	93.20(1)
		SRG/ART-XC		
–	2019-12-11	58828.60	30.8	93.24(3)

[a] barycentric and binary corrections were applied. Orbital parameters were taken from Kühnel et al. (2013)

and with an orbital period of ∼ 250 days (Levine & Corbet 2006; Coe et al. 2007; Kuehnel et al. 2012). The pulsar was discovered in 1993 with the *CGRO* observatory (Stollberg et al. 1993). The neutron star is strongly magnetized with magnetic field of $\sim 8 \times 10^{12}$ G estimated from the cyclotron line discovered around 75–90 keV (Shrader et al. 1999; Yamamoto et al. 2013; Ge et al. 2020).

GRO J1008−57 shows both giant irregular type II outbursts and regular type I outbursts associated with the passage of a neutron star through the periastron. A typical duration of the type I outburst is about 30 days with the maximum luminosity of $L_{\rm X} \sim 10^{37}$ erg s^{-1} (assuming distance to the source of ∼ 5.8 kpc, Riquelme et al. 2012) and decay time of several days. A transition to the regime of the accretion from the cold disk happens around one month after the peak of the outburst when the luminosity drops to $L_{\rm X} \sim 10^{35}$ erg s^{-1} and then remains almost constant slowly decreasing until the next outburst (Tsygankov et al. 2017a).

The most puzzling property of this state in GRO J1008−57 is a significant decrease of the pulsed fraction, which dropped from ∼ 50% in the bright state to below ∼ 20% (upper limit) in the low one (Tsygankov et al. 2017a). Also the spectrum shape in the low state in a wider energy range (above 10 keV) is still unknown, since no sensitive observations in broad energy band were performed until now. In this work we present results of the dedicated observations of GRO J1008−57 in the regime of the accretion from the cold disk done with the *Mikhail Pavlinsky* ART-XC telescope on board the *SRG* mission, and the *NuSTAR* observatory. High quality of the data allowed to detect for the first time the pulsations in such a low state and to trace an evolution of the source broad band spectrum in a wide range of luminosities.

2. OBSERVATIONS AND DATA ANALYSIS

The *SRG* observatory was successively launched to the orbit with the Proton rocket on Jul 13, 2019. The scientific payload includes two X-ray telescopes, eRosita (working energy range of 0.2 − 10 keV) and the *Mikhail Pavlinsky* ART-XC telescope (working energy range of 4 − 30 keV), which are primary designed to carry out the all-sky survey with unprecedented sensitivity.

ART-XC is a grazing incidence focusing X-ray telescope which provides imaging, timing and spectroscopy in the 4-30 keV energy range (Pavlinsky et al. 2021). The telescope consists of seven identical modules with the total effective area of ∼ 450 cm^2 at 6 keV, angular resolution of 45″, energy resolution of 1.4 keV at 6 keV and timing resolution of 23 μs.

During the calibration and performance verification phase (CalPV) conducted soon after the launch, the observatory performed a number of scanning and pointing observations of multiple fields and sources, including GRO J1008−57. This source was observed on Dec 11, 2019 in the pointing mode with the total exposure of 30 ks. The ART-XC telescope was a primary instrument in this observation and worked in a nominal regime. ART-XC data were processed with the analysis software ARTPRODUCTS v0.9 with the CALDB version 20200401. Brief description of the ART-XC analysis software can be found in Pavlinsky et al. (2021).

Preliminary analysis of ART-XC data showed that GRO J1008−57 was significantly detected (Fig. 1 upper panel) with the flux of $\sim 3 \times 10^{-12}$ erg s^{-1} cm^{-2} in the 4 − 12 keV energy band, that is, close to the minimal values registered from the source (Tsygankov et al. 2017a). Pulsations with the period of 93.24 s from the source were confidently detected with ART-XC with ∼ 3σ significance (see middle and bottom panels in Fig. 1). We note that, as shown in the same figure, pulsations with the same period are also detected with *NuSTAR*, where significance of the pulsed signal detection is even higher with false alarm probability of $\sim 2.3 \times 10^{-6}$. It is the first time when pulsations have been detected from the source while in the "cold disk" state. To better characterize spectral and timing properties of the pulsar in the low luminosity state in the broad energy band, we also requested observations with the *NuSTAR* observatory. Thanks to the efforts of the *NuSTAR* team, observations had been carried out just twenty days after the *SRG*/ART-XC pointing. The preliminary analysis showed that between ART-XC and *NuSTAR* observations the source flux was increased by ∼ 30%. Nevertheless considering the slow evolution of flux and spectral parameters of the source quiescence (Tsygankov et al. 2017a), the *SRG*/ART-XC and *NuSTAR* observations can be considered quasi-simultaneous.

The *NuSTAR* observatory consists of two identical X-ray telescope modules, referred to as FPMA and FPMB (Harrison et al. 2013). It provides X-ray imaging, spectroscopy and timing capabilities in the energy range of 3-79 keV. *NuSTAR* performed an observation of GRO J1008−57 on Jan 1, 2020 (ObsID 90501357002) in the state with approximately the same intensity as during the *SRG*/ART-XC observation.

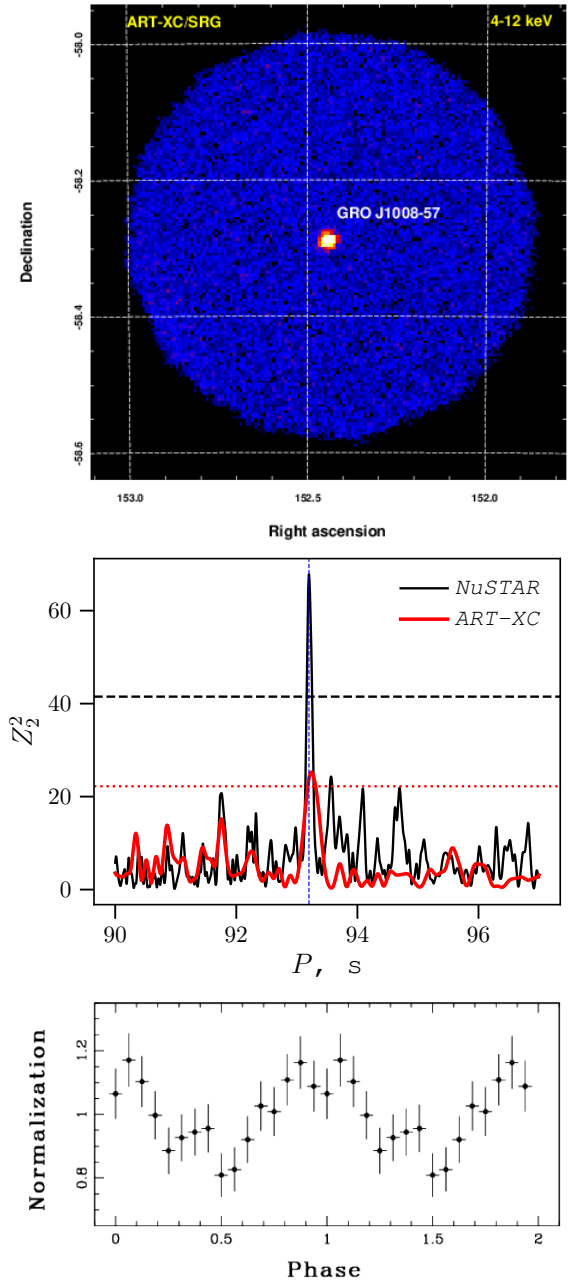

Figure 1. *Upper panel SRG*/ART-XC detection of GRO J1008−57 in the low luminosity state. *middle panel* Z_2^2 periodograms for the *SRG*/ART-XC and *NuSTAR* observations are shown by red and black lines (together with the expected 3σ noise upper limit estimated as described in Brazier (1994) assuming 22% pulsed fraction). *Bottom panel* The source light curve measured with ART-XC in the 4-12 keV energy band and folded with the period of 93.24 s (middle panel).

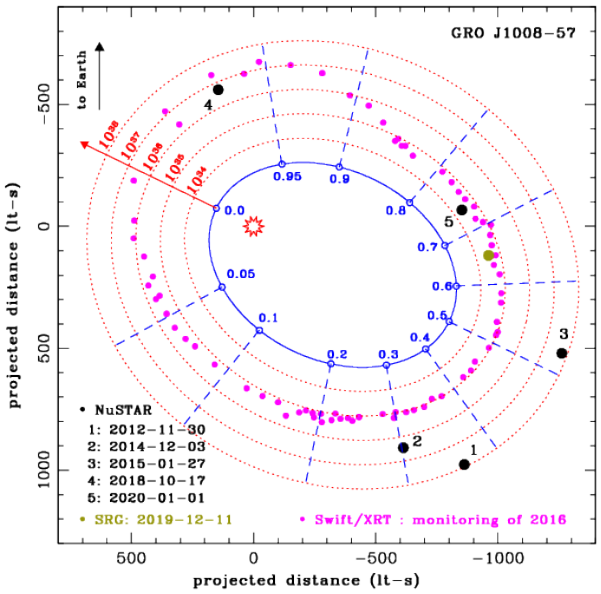

Figure 2. Two-dimensional bolometrically corrected orbital light curve of GRO J1008−57 obtained in 2016 with *Swift*/XRT (magenta filled circles). Bolometric fluxes that were measured with *SRG*/ART-XC and *NuSTAR* observations are shown with light green and black colors points, respectively. Orbital parameters were taken from Kühnel et al. (2013).

To compare spectral and timing properties of GRO J1008−57 in the low state with those during the high state, we also re-analyzed archival *NuSTAR* observations of the source. In particular, observations performed on Nov 30 2012 (ObsID 80001001002), Dec 3 2014 (ObsID 90001003002), Jan 27 2015 (ObsID 90001003004), and Oct 17 2018 (ObsID 90401338002) were used. All *NuSTAR* data were processed with the standard *NuSTAR* Data Analysis Software (NUSTARDAS) v1.8.0 provided under HEASOFT v6.25 with the CALDB version 20200826.

Finally, *Swift*/XRT observed the source simultaneously with *NuSTAR* on Jan 1, 2020 in the photon counting mode with the exposure of ∼ 2 ks (ObsID 00089019001). We used these data to extend the source spectrum into low energies and to compare directly with ART-XC results. Other *Swift*/XRT observations simultaneous with above mentioned *NuSTAR* ones were used to study the broad band spectra of GRO J1008−57. The data were processed using the online tools[1] (Evans et al. 2009) provided by the UK Swift Science Data Centre.

All spectra obtained in four brightest states were grouped to have at least 25 counts per bin using the GRPPHA tool. Spec-

[1] http://www.swift.ac.uk/user_objects/

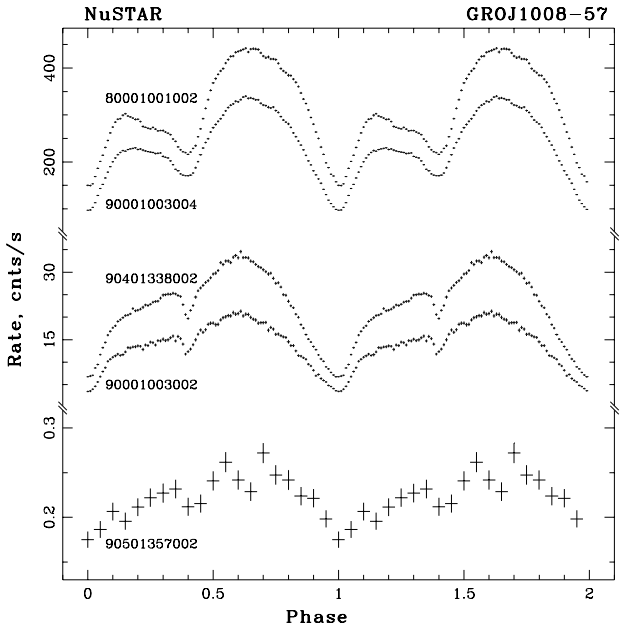

Figure 3. Pulse profiles of GRO J1008−57 as seen by *NuSTAR* in the energy band of 3-79 keV at different luminosities.

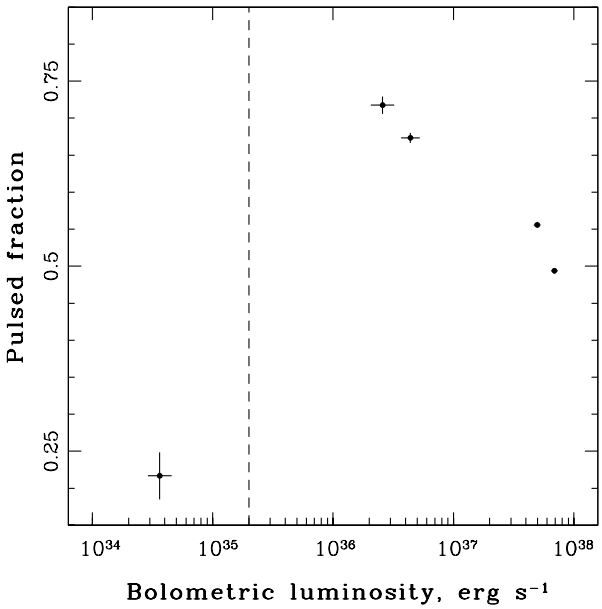

Figure 4. Dependence of the pulsed fraction of GRO J1008−57 in the 3-79 keV energy band as a function of luminosity as observed by *NuSTAR*. Vertical dashed line represents the luminosity $L_{\rm cold} = 2\times10^{35}$ erg s^{-1}, which corresponds to the switch of the accretion to the cold-disk state (Tsygankov et al. 2017a).

tra obtained by *NuSTAR*, *Swift*/XRT and *SRG*/ART-XC in the lowest state were binned to have at least one count per energy bin and modeled using W-statistic (Wachter et al. 1979). The final data analysis (timing and spectral) was performed with the HEASOFT 6.25 software package. All uncertainties are quoted at the 1σ confidence level, if not stated otherwise. Finally, the spectra were also rebinned for plotting in XSPEC.

3. RESULTS

The orbital light curve of GRO J1008−57 showing estimated bolometric luminosity over a full orbital cycle is presented in Fig. 2 (*Swift*/XRT data are adopted from Tsygankov et al. 2017a). Observations with *NuSTAR* and *SRG*/ART-XC are marked by black and light green points, respectively. Note that the observations in Dec, 2019 – Jan, 2020 have been performed around orbital phases 0.65-0.75, where the source luminosity is minimal at a few times 10^{34} erg s^{-1}. Below we discuss the temporal and spectral properties of GRO J1008−57 in the low luminosity state and compare them with those observed at higher luminosities.

3.1. *Timing analysis*

As was already mentioned in the Introduction, pulsations from GRO J1008−57 in the cold-disk state were not detected using *Swift*/XRT and *Chandra* data (Tsygankov et al. 2017a). One of the main goals of our observations was either to find pulsations or to put a more stringent upper limit on the pulsed fraction which was previously estimated at $\sim$ 20% (Tsygankov et al. 2017a).

For the timing analysis both the barycentric and binary corrections were applied to the light curves using the orbital ephemerides reported by Kühnel et al. (2013). As a result we were able to significantly detect pulsations in the low state with the period of $P \simeq 93.2$ s in both *SRG*/ART-XC and *NuSTAR* datasets (see Table 1 and Fig. 1, middle panel). To compare obtained values with measured ones in brighter states and to construct corresponding pulse profiles the same analysis was also performed for other four *NuSTAR* observations. The results are summarized in Table 1. Uncertainties for the pulse period values were determined from the simulated light curves using epoch folding on bootstraped lightcurves as described in detail by Boldin et al. (2013).

The pulse profile of GRO J1008−57 in the bright state exhibits two-peaks structure with a relatively high pulsed fraction. The evolution of the pulse profile as a function of luminosity based on the *NuSTAR* data is presented in Fig. 3. Some minor variations can be observed, mainly in the first peak. However, in spite of three orders of magnitude difference in the observed source flux, the pulse profile shape remains remarkably stable.

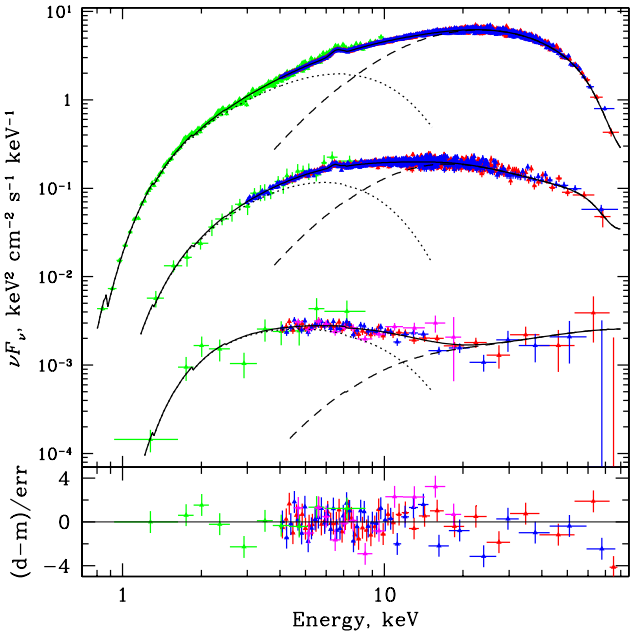

Figure 5. Unfolded spectra of GRO J1008−57 obtained with *NuSTAR* (black and red points), *Swift*/XRT (green points) and *SRG*/ART-XC (magenta points) in different luminosity states. Only three spectra (*NuSTAR* ObsIDs are 80001001002, 900010003004 and 90501357002) of five are shown for clarity. Corresponding residuals for the lowest luminosity state of GRO J1008−57 are shown at the lower panel.

In contrast to that, the pulsed fraction[2] demonstrates more puzzling behaviour as a function of the source luminosity (Fig. 4). It is seen from the figure, that in the bright state the pulse fraction has relatively high values depending on the flux from $\sim$ 70% to $\sim$ 50%. Moreover, at high luminosity levels it also appears to anti-correlate with the flux, which is typical for the majority of XRPs in the hard X-ray band (Lutovinov & Tsygankov 2009). However, at some luminosity (probably coinciding with the transitional luminosity to the cold-disk accretion, although available data does not allow to determine this time accurately) this dependence breaks down resulting in a very strong drop of the pulsed fraction to 22 ± 3%. Note, that the pulsed fraction measured by *SRG*/ART-XC in the 4-12 keV energy range is approximately the same 20 ± 5%.

3.2. *Spectral analysis*

Spectra of XRPs provide an important information about the physical mechanisms of the formation of the radiation under extreme conditions in the vicinity of neutron stars and its subsequent interaction with the surrounding matter in strong magnetic fields. These processes are quite complex and not fully understood yet, which makes it difficult to develop physically motivated spectral models.

Therefore, spectra of XRPs have long been described by one-component phenomenological models (such as a power law with a high energy exponential cutoff, a.k.a. HIGHCUT or CUTOFFPL in XSPEC), modified by the absorption at lower energies and, in some cases, by the cyclotron absorption lines (see, e.g., White et al. 1983; Coburn et al. 2002; Filippova et al. 2005; Walter et al. 2015). Expanding the available energy range and increasing the sensitivity of modern instruments made it possible to study spectra of accreting neutron stars in a wide range of luminosities including periods of quiescence. It required the development of new approaches to the analysis of the spectral information and the use of multicomponent models to describe the continuum, although, as before, these models largely remain phenomenological.

The observed spectrum of GRO J1008−57 was usually described with the aforementioned phenomenological models, like a cutoff power-law, Fermi–Dirac cutoff powerlaw, or combination of negative and positive powerlaws with an exponential cutoff (see, e.g., Coe et al. 2007; Yamamoto et al. 2014) modified by additional components to account for the interstellar absorption, soft excess, fluorescent iron line and cyclotron line around 80 keV (see, e.g., Kühnel et al. 2013; Bellm et al. 2014).

Recent measurements of the GRO J1008−57 broadband spectrum during an outburst with the *HMXT* observatory showed that it can be described by two-components (power law with high-energy exponential cutoff plus black body) absorbed continuum model with the cyclotron absorption line at the energy of $\sim$ 90 keV (Ge et al. 2020). It is important to note that the line was robustly detected and its parameters were measured with very high significance.

Following previous works, we tried to describe the continuum of the source in a wide range of luminosities with a combination of two components. All of these combinations were modified by the low-energy absorption in the form of PHABS model in the XSPEC package and by the cyclotron absorption line (in the form of the GABS model in the XSPEC package) with the energy and width fixed at values obtained by (Ge et al. 2020). The line depth was a free parameter. Formally, the line energy is outside of the working energy range of the *NuSTAR* observatory, but due to the significant width and depth the absorption feature affects the cutoff energy and thus need to be included in the model.

We fitted the source continuum spectra with different combination of XSPEC models previously used by other authors: BBODY+HIGHCUT , BBODY+CUTOFFPL, HIGHCUT + GAUSSIAN, HIGHCUT + COMPTT, BBODY+COMPTT, COMPTT+COMPTT. It was found that the combination of the two Comptonization components best describes the source spectrum in all states. Note, that

[2] defined as PF = $(F_{max} - F_{min})/(F_{max} + F_{min})$, where F_{max} and F_{min} are maximum and minimum fluxes in the pulse profile, respectively

Table 2. Best-fitting results for the GRO J1008−57 broadband spectra in different luminosity states

Parameter[a]	Low-energy part	High-energy part
	80001001002	
T_0, keV	0.30 ± 0.05	3.19 ± 0.15
T_p, keV	1.89 ± 0.05	8.87 ± 0.15
τ_p	12.8 ± 0.3	3.73 ± 0.12
N_H	1.14 ± 0.10	
E_{Fe}, keV	6.55 ± 0.01	
σ_{Fe}, keV	0.28 ± 0.01	
τ_{cyc},	1.23 ± 0.18	
C_B	1.030 ± 0.001	
C_{XRT}	1.132 ± 0.005	
F_X, erg s^{-1} cm^{-2}	2.08×10^{-8}	
χ^2 (d.o.f.)	1.07 (3236)	
	90001003004	
T_0, keV	0.28 ± 0.06	4.28 ± 0.25
T_p, keV	2.22 ± 0.06	12.0 ± 1.4
τ_p	11.87 ± 0.30	2.24 ± 0.41
N_H	1.36 ± 0.09	
E_{Fe}, keV	6.59 ± 0.01	
σ_{Fe}, keV	0.28 ± 0.01	
τ_{cyc},	2.14 ± 0.36	
C_B	1.015 ± 0.001	
C_{XRT}	1.297 ± 0.006	
F_X, erg s^{-1} cm^{-2}	1.50×10^{-8}	
χ^2 (d.o.f.)	1.10 (2702)	
	90401338002	
T_0, keV	0.33 ± 0.53	3.36 ± 0.20
T_p, keV	1.73 ± 0.07	14.8 ± 2.7
τ_p	13.8 ± 3.6	1.7 ± 0.4
N_H	1.45 ± 0.71	
E_{Fe}, keV	6.34 ± 0.02	
σ_{Fe}, keV	0.2 (fix)	
τ_{cyc},	1.83 ± 0.56	
C_B	1.034 ± 0.002	
F_X, erg s^{-1} cm^{-2}	1.34×10^{-9}	
χ^2 (d.o.f.)	1.01 (1783)	
	90001003002	
T_0, keV	0.74 ± 0.23	3.20 ± 0.32
T_p, keV	1.76 ± 0.27	20 ± 16
τ_p	11.8 ± 4.1	1.2 ± 1.2
N_H	0.66 ± 0.29	
E_{Fe}, keV	6.4 (fix)	
σ_{Fe}, keV	0.2 (fix)	
τ_{cyc},	0.8 ± 1.0	
C_B	1.027 ± 0.004	
C_{XRT}	1.120 ± 0.042	
F_X, erg s^{-1} cm^{-2}	8.11×10^{-10}	
χ^2 (d.o.f.)	1.00 (1356)	
	90501357002	
T_0, keV	0.25 ± 0.53	> 5
T_p, keV	3.5 ± 3.1	23 ± 19
τ_p	4.4 ± 1.6	> 5.5
N_H	2.5 ± 1.5	
C_B	1.042 ± 0.022	
C_{XRT}	0.84 ± 0.11	
C_{ART-XC}	0.65 ± 0.02	
F_X, erg s^{-1} cm^{-2}	1.50×10^{-11}	
χ^2 (d.o.f.)	1.01 (1592)	

[a] Here T_p, τ_p and T_0 are the plasma temperature, plasma optical depth, temperature of the seed photons for the COMPTT model. Fluxes are given in the 0.5–100 keV energy range.

earlier two Comptonization components were proposed by Ferrigno et al. (2009) to fit the spectra of super-critical X-ray pulsar 4U 0115+63 where the model was motivated to account for the influence of bulk and thermal Comptonization in accretion column supported by radiation pressure (Becker & Wolff 2007). This model, however, is not applicable in the case of sub-critical accretion, which considered in this paper.

To take into account a strong emission feature associated with the fluorescent iron emission line around 6.4 keV, a corresponding component in the Gaussian form was added also to the model in line with the photo-absorption and cyclotron resonant scattering feature discussed above. The final best-fit parameters (including model flux) are summarized in Table 2. The energy spectra of GRO J1008−57 are shown in Fig. 5.

The source and background spectra from both the FPMA and FPMB modules of *NuSTAR* as well as from the *Swift*/XRT and *SRG*/ART-XC telescopes were used for simultaneous fitting. To take into account the uncertainty in the *NuSTAR* modules calibrations and potentially slightly different source flux during the (not strictly simultaneous) observations by different observatories, cross-calibration constants between them were included in all spectral models. The C_B, C_{XRT} and C_{ART-XC} constants from Table 2 correspond to the cross-calibrations of the FPMB module, the XRT telescope to the FPMA module and the ART-XC telescope to the FPMA module, respectively. The value of C_{ART-XC} reflects the source flux change between ART-XC and *NuSTAR* observations connected either with its slow brightening towards the next outburst or with its local short-term variability. Nevertheless the spectrum remains practically unchanged that allow us to fit ART-XC and *NuSTAR* data simultaneously.

4. DISCUSSION AND CONCLUSION

In this work we presented results of the first dedicated broadband observations of GRO J1008−57 in the low state using data of *NuSTAR* and *SRG*/ART-XC. Timing analysis

from both instruments resulted in the significant detection of pulsations from the source with the pulsed fraction of ∼ 20%, that is several times lower than in the bright state.

One of the possible explanation of such a behaviour is an increase of the emitting region on the NS surface as a result of the deeper penetration of the cold disk into the pulsar magnetosphere. More detailed discussion of that requires model of the interaction of the cold disk with magnetic field and is out of scope of the current paper.

Another possibility is related to the structure of a NS atmosphere at low mass accretion rates. According to numerical simulations, the upper layer of the atmosphere is overheated up to temperatures ∼ 100 keV (Suleimanov et al. 2018; Mushtukov et al. 2020). The photons which leave the atmosphere at larger angles to the normal are originated (or experience the last scattering) from smaller optical depth in the atmosphere. In the case of temperature increasing with the optical depth, the intensity of radiation tends to be larger along the normal. In the case of the inverse temperature structure (when the upper layers are hotter than the underlying ones), the intensity increases with the angle to the normal and, thus, the beam pattern generated by a hot spot with an overheated upper layer is expected to be compressed in the direction perpendicular to the stellar surface. Such a modification of the beam pattern can result in a reduction of the pulsed fraction.

The qualitative similarity of the pulse profiles (see Fig. 3) in different luminosity states allows us to speculate that in all cases, we see the source in the same regime of accretion (Basko & Sunyaev 1976; Gnedin & Sunyaev 1973; Mushtukov et al. 2015). Accounting for a strong magnetic field strength at the NS surface, we conclude that the source is still in a sub-critical regime even at $L \sim 10^{38}$ erg s^{-1}. It puts valuable limitations to the critical luminosity at extremely strong field strength: $L_{\rm crit} > 10^{38}$ erg s^{-1} for $B \simeq 7 \times 10^{12}$ G.

We were able for the first time to trace the evolution of the broadband spectrum of the source on a scale of three orders of magnitude in luminosity. It was shown that in all states it can be adequately described by a two-component model with a clear division of the components into soft and hard ones. The spectrum in the high state is in good agreement with the results of previous studies, in which the classical 'power-law with high energy cutoff' model and an additional blackbody component was used. At the lowest state, the spectrum shape becomes a double-hump one. Such a shape is already proved to be typical for XRPs with low mass accretion rate (Doroshenko et al. 2012; Tsygankov et al. 2019b,a; Doroshenko et al. 2021). The tentative peak energy of the hard spectral component is consistent with the position of the cyclotron line at about 80–90 keV, but its temperature is not limited due to low statistics. This is in line with the explanation of this component due to the emission of cyclotron photons in the NS atmosphere caused by collisional excitation of electrons to upper Landau levels and consequent Comptonization by hot electron gas (Mushtukov et al. 2020).

ACKNOWLEDGEMENTS

We thanks to the *NuSTAR* team for organising prompt observations. This work was financially supported by the Russian Science Foundation (grant 19-12-00423).

REFERENCES

Bachetti, M., Harrison, F. A., Walton, D. J., et al. 2014, Nature, 514, 202, doi: 10.1038/nature13791

Basko, M. M., & Sunyaev, R. A. 1976, MNRAS, 175, 395, doi: 10.1093/mnras/175.2.395

Becker, P. A., & Wolff, M. T. 2007, ApJ, 654, 435, doi: 10.1086/509108

Bellm, E. C., Fürst, F., Pottschmidt, K., et al. 2014, ApJ, 792, 108, doi: 10.1088/0004-637X/792/2/108

Boldin, P. A., Tsygankov, S. S., & Lutovinov, A. A. 2013, Astronomy Letters, 39, 375, doi: 10.1134/S1063773713060029

Brazier, K. T. S. 1994, MNRAS, 268, 709, doi: 10.1093/mnras/268.3.709

Campana, S., Stella, L., Israel, G. L., et al. 2002, ApJ, 580, 389, doi: 10.1086/343074

Coburn, W., Heindl, W. A., Rothschild, R. E., et al. 2002, ApJ, 580, 394, doi: 10.1086/343033

Coe, M. J., Bird, A. J., Hill, A. B., et al. 2007, MNRAS, 378, 1427, doi: 10.1111/j.1365-2966.2007.11878.x

Doroshenko, V., Santangelo, A., Doroshenko, R., et al. 2014, A&A, 561, A96, doi: 10.1051/0004-6361/201322472

Doroshenko, V., Santangelo, A., Kreykenbohm, I., & Doroshenko, R. 2012, A&A, 540, L1, doi: 10.1051/0004-6361/201218878

Doroshenko, V., Santangelo, A., Tsygankov, S. S., & Long, J. 2021, A&A, submitted

Doroshenko, V., Zhang, S. N., Santangelo, A., et al. 2020, MNRAS, 491, 1857, doi: 10.1093/mnras/stz2879

Evans, P. A., Beardmore, A. P., Page, K. L., et al. 2009, MNRAS, 397, 1177, doi: 10.1111/j.1365-2966.2009.14913.x

Ferrigno, C., Becker, P. A., Segreto, A., Mineo, T., & Santangelo, A. 2009, A&A, 498, 825, doi: 10.1051/0004-6361/200809373

Filippova, E. V., Tsygankov, S. S., Lutovinov, A. A., & Sunyaev, R. A. 2005, Astronomy Letters, 31, 729, doi: 10.1134/1.2123288

Fürst, F., Walton, D. J., Harrison, F. A., et al. 2016, ApJL, 831, L14, doi: 10.3847/2041-8205/831/2/L14

Ge, M. Y., Ji, L., Zhang, S. N., et al. 2020, ApJL, 899, L19, doi: 10.3847/2041-8213/abac05

Gnedin, Y. N., & Sunyaev, R. A. 1973, A&A, 25, 233

Harrison, F. A., Craig, W. W., Christensen, F. E., et al. 2013, ApJ, 770, 103, doi: 10.1088/0004-637X/770/2/103

Israel, G. L., Belfiore, A., Stella, L., et al. 2017, Science, 355, 817, doi: 10.1126/science.aai8635

Kuehnel, M., Mueller, S., Kreykenbohm, I., et al. 2012, The Astronomer's Telegram, 4564, 1

Kühnel, M., Müller, S., Kreykenbohm, I., et al. 2013, A&A, 555, A95, doi: 10.1051/0004-6361/201321203

Levine, A. M., & Corbet, R. 2006, The Astronomer's Telegram, 940, 1

Lutovinov, A. A., & Tsygankov, S. S. 2009, Astronomy Letters, 35, 433, doi: 10.1134/S1063773709070019

Lutovinov, A. A., Tsygankov, S. S., Karasev, D. I., Molkov, S. V., & Doroshenko, V. 2019, MNRAS, 485, 770, doi: 10.1093/mnras/stz437

Lutovinov, A. A., Tsygankov, S. S., Krivonos, R. A., Molkov, S. V., & Poutanen, J. 2017, ApJ, 834, 209, doi: 10.3847/1538-4357/834/2/209

Mushtukov, A. A., Suleimanov, V. F., Tsygankov, S. S., & Portegies Zwart, S. 2020, arXiv e-prints, arXiv:2006.13596. https://arxiv.org/abs/2006.13596

Mushtukov, A. A., Suleimanov, V. F., Tsygankov, S. S., & Poutanen, J. 2015, MNRAS, 447, 1847, doi: 10.1093/mnras/stu2484

Pavlinsky, M., Tkachenko, A., Levin, V., & et al. 2021, A&A, submitted

Riquelme, M. S., Torrejón, J. M., & Negueruela, I. 2012, A&A, 539, A114, doi: 10.1051/0004-6361/201117738

Rodríguez Castillo, G. A., Israel, G. L., Belfiore, A., et al. 2020, ApJ, 895, 60, doi: 10.3847/1538-4357/ab8a44

Semena, A. N., Lutovinov, A. A., Mereminskiy, I. A., et al. 2019, MNRAS, 490, 3355, doi: 10.1093/mnras/stz2722

Shrader, C. R., Sutaria, F. K., Singh, K. P., & Macomb, D. J. 1999, ApJ, 512, 920, doi: 10.1086/306785

Stollberg, M. T., Finger, M. H., Wilson, R. B., et al. 1993, IAUC, 5836, 1

Suleimanov, V. F., Poutanen, J., & Werner, K. 2018, A&A, 619, A114, doi: 10.1051/0004-6361/201833581

Tsygankov, S. S., Doroshenko, V., Mushtukov, A. A., et al. 2019a, MNRAS, 487, L30, doi: 10.1093/mnrasl/slz079

Tsygankov, S. S., Lutovinov, A. A., Doroshenko, V., et al. 2016, A&A, 593, A16, doi: 10.1051/0004-6361/201628236

Tsygankov, S. S., Mushtukov, A. A., Suleimanov, V. F., et al. 2017a, A&A, 608, A17, doi: 10.1051/0004-6361/201630248

Tsygankov, S. S., Rouco Escorial, A., Suleimanov, V. F., et al. 2019b, MNRAS, 483, L144, doi: 10.1093/mnrasl/sly236

Tsygankov, S. S., Wijnands, R., Lutovinov, A. A., Degenaar, N., & Poutanen, J. 2017b, MNRAS, 470, 126, doi: 10.1093/mnras/stx1255

Wachter, K., Leach, R., & Kellogg, E. 1979, ApJ, 230, 274, doi: 10.1086/157084

Walter, R., Lutovinov, A. A., Bozzo, E., & Tsygankov, S. S. 2015, A&A Rv, 23, 2, doi: 10.1007/s00159-015-0082-6

White, N. E., Swank, J. H., & Holt, S. S. 1983, ApJ, 270, 711, doi: 10.1086/161162

Wijnands, R., & Degenaar, N. 2016, MNRAS, 463, L46, doi: 10.1093/mnrasl/slw096

Yamamoto, T., Mihara, T., Sugizaki, M., et al. 2014, PASJ, 66, 59, doi: 10.1093/pasj/psu028

—. 2013, The Astronomer's Telegram, 4759, 1